2011

Mass and relative elution time profiling: Two-dimensional analysis of sphingolipids in Alzheimer's disease brains

Leila Hejazi
University of New South Wales

Jason Wong
University of New South Wales

D. Cheng
Neuroscience Research Australia

Nicholas Proschogo
University of New South Wales

D. Ebrahimi
University of New South Wales

See next page for additional authors

Mass and relative elution time profiling: Two-dimensional analysis of sphingolipids in Alzheimer's disease brains

Abstract

Current lipidomic profiling methods rely mainly on MS to identify unknown lipids within a complex sample. We describe a new approach, involving LC×MS/MS (liquid chromatography×tandem MS) analysis of sphingolipids based on both mass and hydrophobicity, and use this method to characterize the SM (sphingomyelin), ceramide and GalCer (galactosylceramide) content of hippocampus from AD (Alzheimer's disease) and control subjects. Using a mathematical relationship we exclude the influence of sphingolipid mass on retention time, and generate two-dimensional plots that facilitate accurate visualization and characterization of the different ceramide moieties within a given sphingolipid class, because related molecules align horizontally or vertically on the plots. Major brain GalCer species that differ in mass by only 0.04 Da were easily differentiated on the basis of their hydrophobicity. The importance of our method's capacity to define all of the major GalCer species in the brain samples is illustrated by the novel observation that the proportion of GalCer with hydroxylated fatty acids increased approximately 2-fold in the hippocampus of AD patients, compared with age- and gender-matched controls. This suggests activation of fatty acid hydroxylase in AD. Our method greatly improves the clarity of data obtained in a lipid profiling experiment and can be expanded to other lipid classes.

Disciplines

Medicine and Health Sciences

Publication Details

Hejazi, L., Wong, J. W. H., Cheng, D., Proschogo, N., Ebrahimi, D., Garner, B. & Don, A. S. (2011). Mass and relative elution time profiling: Two-dimensional analysis of sphingolipids in Alzheimer's disease brains. Biochemical Journal, 438 (1), 165-175.

Authors

Leila Hejazi, Jason Wong, D. Cheng, Nicholas Proschogo, D. Ebrahimi, Brett Garner, and Anthony Don

Mass and Relative Elution Time Profiling: Two-dimensional Analysis of Sphingolipids in Alzheimer's Disease Brains

Leila Hejazi[*†], Jason W.H. Wong[‡†], Danni Cheng[§], Nick Proschogo[‖], Diako Ebrahimi[‖], Brett Garner[¶], Anthony S. Don[‡1]

[*]Bioanalytical Mass Spectrometry Facility, Mark Wainwright Analytical Centre, [‡]Lowy Cancer Research Centre, Prince of Wales Clinical School, and [‖]Centre for Vascular Research, Faculty of Medicine, University of New South Wales, Sydney, NSW 2052, Australia,
[§]Neuroscience Research Australia, Sydney, NSW 2031, Australia,
[¶]Illawarra Health and Medical Research Institute, School of Biological Sciences, University of Wollongong, Wollongong, NSW 2522, Australia
[†]These authors contributed equally

Running head: Mass and Relative Elution Time Profiling of Sphingolipids

[1]Address correspondence to: Dr Anthony Don, Level 2 C25 Lowy Cancer Research Centre, University of New South Wales, Sydney, NSW, 2052, Australia. Ph: +612 9385 1387. Fax: +612 9385 1510. email: anthonyd@unsw.edu.au

Synopsis
Current lipidomic profiling methods rely mainly on mass spectrometry to identify unknown lipids within a complex sample. We describe a new approach, involving LC×MS/MS analysis of sphingolipids based on both mass and hydrophobicity, and use this method to characterize the sphingomyelin (SM), ceramide, and galactosylceramide (GalCer) content of hippocampus from Alzheimer's Disease (AD) and control subjects. Using a mathematical relationship we exclude the influence of sphingolipid mass on retention time, and generate two-dimensional plots that facilitate accurate visualization and characterization of the different ceramide moieties within a given sphingolipid class, because related molecules align horizontally or vertically on the plots. Major brain GalCer species that differ in mass by only 0.04 Da were easily differentiated on the basis of their hydrophobicity. The importance of our method's capacity to define all of the major GalCer species in the brain samples is illustrated with the novel observation that the proportion of GalCer with hydroxylated fatty acids increased approximately two-fold in the hippocampus of AD patients, compared to age- and gender-matched controls. This suggests activation of fatty acid hydroxylase in AD. Our method greatly improves the clarity of data obtained in a lipid profiling experiment and can be expanded to other lipid classes.

Key Words
sphingolipids, ceramide, cerebroside, galactosylceramide, Alzheimer's Disease, lipidomic

Abbreviations
AD, Alzheimer's Disease; GluCer, glucosylceramide; GalCer, galactosylceramide; HFA, hydroxylated fatty acid; LC, liquid chromatography; MRM, multiple reaction monitoring; MS, mass spectrometry; NFA, normal fatty acid; RT, retention time; SM, sphingomyelin; TIC, total ion chromatogram.

INTRODUCTION

The sphingolipids are a diverse family of structural and signaling lipids that have a broad range of functions in normal physiology and pathology [1, 2]. Altered sphingolipid metabolism has been implicated in the pathology of cancer [2], cardiovascular diseases [3], type II diabetes [4], and

neurodegenerative diseases such as Parkinson's disease [5] and AD [6]. The common constituent of all sphingolipids is the sphingoid base, which in mammals is most commonly 18-carbon sphingosine or dihydrosphingosine. A family of six ceramide synthases catalyze the transfer of fatty acids to the amine group of sphingosine or dihydrosphingosine, forming the central sphingolipid metabolite ceramide (Figure 1a). The fatty acids vary in length from 14 to 26 carbons, may contain one or more double bonds, and may be hydroxylated. These variations create significant structural and biophysical heterogeneity within ceramides. Addition of different headgroups to the primary hydroxyl of ceramides gives rise to the different classes of sphingolipids, which are all built on a ceramide lipid "backbone".

Ceramide is itself a signaling molecule that is frequently associated with execution of apoptosis [2], but also plays a role in establishing epithelial cell polarity [7] and the formation of cell-cell junctions [8]. The abundant plasma membrane lipid SM is formed by the transfer of a phosphatidylcholine headgroup onto ceramide (Figure 1a). The interaction of SM with cholesterol gives rise to lipid rafts, specialized regions of the plasma membrane where cell signaling platforms are formed. Alternatively, glucose, galactose, or phosphate headgroups may be transferred onto ceramide, giving rise to lipid mediators with distinct functions. GalCer may be sulfated (forming sulfatide), and both of these lipids are major constituents of myelin. Accordingly, GalCer synthesis is critical for normal brain function [9, 10].

The aim of this research project was to develop a two-dimensional (2D) sphingolipid profiling approach, in which the lipids are separated and identified on the basis of both mass and hydrophobicity. Sphingolipids in biological samples are usually quantified using Liquid Chromatography-tandem Mass Spectrometry (LC-MS/MS). In general, a defined number of lipid metabolites are quantified by running the mass spectrometer in Multiple Reaction Monitoring (MRM) mode, in which a specific precursor and product ion mass are used to identify each metabolite of interest, which is quantified relative to external standards [11, 12]. However, MRM assumes prior knowledge about which lipids are present in a given extract. A more objective profiling approach can be achieved by scanning for precursor ions within a defined mass range, whilst monitoring for product ions that are characteristic of a particular lipid backbone, e.g. sphingosine (*m/z* 264) or dihydrosphingosine (*m/z* 266) [12]. Lipids identified using this approach may then be quantified more accurately in a follow-up MRM experiment. However, assigning a molecular structure to a given lipid based only on its precursor and product masses is not always feasible, because a given mass can often be assigned to two or more biologically relevant structures.

Incorporating an LC step prior to MS/MS improves sensitivity by removing interfering ions, separating out different lipid components in the cell or tissue extract, and concentrating each lipid species into a narrow elution time window. In theory, the incorporation of an LC column prior to MS can also provide biochemical information that helps to definitively assign a structure to a given precursor and product mass. However, LC is not used in mass scanning/profiling experiments, firstly because column Retention Time (RT) is not informative unless referenced to structurally defined standards; and secondly because in reverse phase chromatography of lipids with the same headgroup, differences in mass conferred by different acyl chain lengths have a large impact on RT. To effectively use RT in the characterization of unknown lipids from a lipid profiling experiment, we first needed to develop a method in which RT is made independent of N-acyl chain length, and therefore mass. To do this we adapted and modified a method that was used for separation of hydrocarbons [13, 14] and fatty acid methyl esters [15, 16].

We describe here an LC×MS/MS approach (as distinct from an LC-MS/MS approach) for characterization of sphingolipids in complex biological extracts that we refer to as Mass and Relative Elution Time (MRET) profiling. After excluding the influence of mass on RT for any given class of sphingolipid, the resulting 2D plots can be used to predict the number and position of double bonds within the lipid tails, and the presence of functional groups such as hydroxyls, without any need for

chemical derivatization of the lipids or the use of high resolution mass analyzers. We describe how this approach can be used to collate the MS output of brain tissue extracts from twelve different human subjects, forming 2D plots of the SM, ceramide, and GalCer content that also incorporate a semi-quantitative measure of relative abundance for each distinct metabolite. These plots are an informative and versatile way to visualize complex lipidomic data sets. Importantly, we show how this approach allows us to distinguish between GalCer species that are structurally and biochemically different, but can not be distinguished on the basis of precursor and product ion mass.

EXPERIMENTAL

Liquid Chromatography and Mass Spectrometry

LC-MS/MS was performed on a Thermo TSQ triple quadrupole mass spectrometer, operating in positive ion mode, coupled to a 3 x 150 mm Agilent XDB-C8 column (5 micron pore size) on an Accela UPLC system (Thermo). In both methods, lipids were separated using a binary gradient program, at a flow rate of 0.5 mL/min: mobile phase A was 0.2% formic acid/2 mM ammonium formate in water; mobile phase B was 0.2% formic acid/1 mM ammonium formate in methanol. The HPLC gradient for separation of ceramide and GalCer was as follows: 0 min, 20:80 A/B; 2 min, 15:85 A/B; 3min, 10:90 A/B; 4 min, 1:99 A/B; 5 min 0:100 A/B; 18 min 0:100 A/B; 20 min 20:80 A/B. C18 chromatography was performed on a 2 x 150 mm Phenomenex C18 column (3 micron pore size). The gradient employed was: 0 min, 10:90 A/B; 2 min, 0/100 A/B; 43 min, 0/100 A/B; 45 min, 10/90 A/B. The HPLC gradient for separation of SM (on the C8 column) was: 0 min, 20:80 A/B; 2 min, 10:90 A/B; 3 min, 1:99 A/B; 19 min, 1/99 A/B; 20 min, 20:80 A/B; 22 min, 20:80 A/B.

Ceramide and GalCer were analyzed simultaneously by precursor ion scanning over the mass range 450 to 1050 Da, monitoring for *m/z* 262.0, 264.1, and 266.1 product ions at collision energy 30 eV. For clarity this paper describes results derived primarily from the *m/z* 264 product ion scan. Scan time was one second for each event (i.e. each scan was run every three seconds). SM species were detected separately, monitoring for an *m/z* 184 product ion at collision energy 35 eV. For ceramide standards run over a broad concentration range, from 8 nM to 8 μM (total 6 concentrations), in precursor scanning mode, Coefficient of Variation (CV) in *m/z* of LC peaks ranged from 0.005 to 0.06, whilst CV in RT ranged from 0.018 to 0.407. Variation in retention time between the start and the end of a sequence of 18 samples (i.e. 6 hours apart) was less than 1% for three different GalCer standards: d18:1/12:0, RT = 6.88 and 6.88 min; d18:1/18:0, RT = 8.42 and 8.36 min; d18:1/24:1, RT = 10.39 and 10.33 min. For lipid detection in MRM mode, the TSQ was set to monitor a list of events as shown in Table 1, each with a scan time of 0.06 seconds. Note that mass accuracy for the Quantum TSQ is ± 0.5 Da.

High mass accuracy analysis of GalCer species was performed using an LTQXL Orbitrap Mass Spectrometer operating in positive [electrospray] mode, connected to an Accela liquid chromatography system (Thermo Scientific). The gradient program, at flow rate 0.4 mL/min, was as follows: 0 min, 20:80 A/B; 2.5 min, 15:85 A/B; 3.8min, 10:90 A/B; 5 min, 1:99 A/B; 6.5 min 0:100 A/B; 30 min 0:100 A/B; 32 min 20:80 A/B. Mass spectra were recorded in Fourier Transform full scan mode, mass range 80 - 1100 Da, mass resolution 60000 (m/Δm, FWHM at 400 Da).

Lipid Extraction from Human Brain Tissue

Human brain tissues were obtained from the Sydney Brain Bank and the New South Wales Tissue Resource Centre. Ethics approval for the current study was from the University of Wollongong Human Research Ethics Committee (HE10/327). Tissue samples were obtained from brains of six AD patients, clinically and pathologically defined using NIA-Reagan criteria, and six age- and gender-matched controls [17]. These 12 samples have been used in another, unrelated study [18]. Clinical information for each case including gender, age at death, post-mortem interval (PMI), and clinical

cause of death is provided in Table 2. Frozen brain tissue from the hippocampus and cerebellum was pulverized over dry ice and stored at -80°C until required for analysis.

Lipids were extracted from approximately 10 mg frozen brain tissue, using a modification of the single phase extraction method described by Bielawski et al [19]. A 1.5 mL mixture of ethyl acetate:isopropanol:water (30:10:60, v/v/v) (solution A), together with 1.5 mL chloroform/methanol (1:2) (solution B), was added to the frozen brain tissue in a 15 mL glass tube. A 50 μL cocktail of internal standards was added, comprising 5 μM each of d18:1/17:0 ceramide, d18:1/12:0 SM, and d18:1/12:0 GalCer. The brain tissue was further crushed with a dounce homogenizer, sonicated for 2 h in a Unisonics FXP10M water bath and incubated, with occasional sonicating, for 10 h at 35 °C to extract sphingolipids [12]. The extract was centrifuged for 10 min at 3700×g (25°C), and the supernatant transferred to a clean glass tube. The residue was re-extracted with 1.5 mL solution A as described above, then 1 mL chloroform/methanol (2:1). The supernatants from each extraction step were combined, divided into two parts, then dried down in a Thermo SC210 Speedvac. One half of the extract was reconstituted in 200 μL HPLC mobile phase (80:20 A/B), vortexed thoroughly, and centrifuged at 3700×g for 5 min (25°C). The supernatant was transferred to an HPLC vial with 200 μL glass insert, and stored at –20°C until LC-MS/MS analysis of ceramide and GalCer/GluCer content. The other half of the extract was further processed for SM analysis, exactly as described previously [19]. Note that for SM preparation an alkaline hydrolysis step is included to remove phosphatidylcholine, which is highly abundant and may interfere with SM analysis. Analytical (HPLC) grade solvents were purchased from Merck. All lipid standards were purchased from Avanti Polar Lipids, except for SM(d18:1/22:0), which was from Matreya LLC.

Data extraction and collation from multiple samples

LC-MS/MS data from each sample was converted to mzXML file format using ReAdW (version 4.3.1) [20] with default parameters. The data was then processed using in-house software: Mass spectra were de-isotoped based on the detection of estimated mass-dependent isotope profiles. In this process, the intensity of all isotopic peaks is combined into a single monoisotopic peak. Furthermore, water loss events (-18±0.25 *m/z*) were also removed from each spectrum. Peaks were then detected in each spectrum within the LC-MS/MS run. We defined a peak as ions with an intensity of greater than 2.5% of the base peak and with at least 10,000 ion counts. To eliminate redundancy, all peaks with a similar mass (±0.25 *m/z*) and retention time (±0.5 minutes) arising from the same transition events across the chromatogram were culled, with the most intense peak within each mass and retention time window retained. To determine the abundance of a peak within a sample, the selected ion chromatogram is computed with a mass window of ± 0.25 *m/z* and smoothed using the Savitzky-Golay filter [21] before the area under the chromatogram was calculated. This procedure results in a final list of peaks and their corresponding abundance for each selected reaction monitoring event. For MRM experiments, the precursor mass was used directly from each monitored event.

For sample comparison, peak lists generated from each sample were further compiled to generate a list of peaks with aligned mass and retention times. The alignment process is based on the use of mass and retention time windows (± 0.5 *m/z* and ± 0.5 min, respectively). For the SM analysis, the retention time window was increased to ± 1.0 min to accommodate broader elution peaks, and to account for chromatographic variation between analyses which were performed over several days. We did not find it necessary to apply sophisticated non-linear alignment procedures [22].

This software tool is implemented using C++ and is available to the research community as a web resource, located at http://www.cancerresearch.unsw.edu.au/crcweb.nsf/page/lipidms. Source code will be made available to non-commercial users upon request.

Data Processing for 2D plots and Lipid Quantification

The RT vs *m/z* data for d18:1/(12:0, 14:0, 16:0, 18:0, 20:0, 22:0, and 24:0) ceramide standards was fitted to a centered second order polynomial equation, given by $y = 9.423 + 0.0353(x – 566.5) + 0.000133(x - 566.5)^2$ using GraphPad PRISM ($R^2 = 0.9994$). For C18 chromatography, the relationship between *m/z* and RT was also quadratic, given by $y = 9.610 + 0.09921(x – 576.7) + 0.0005569(x – 576.7)^2$; $R^2 = 0.9987$. This equation was then used to derive a theoretical RT for all *m/z* values. The theoretical RT was subtracted from the observed RT, yielding the relative RT (which is approximately 0 for all points used to fit the curve). There were insufficient commercially available GalCer and SM standards to derive the RT vs *m/z* relationship. We therefore extracted the *m/z* and RT for GalCer and SM bearing saturated N-acyl chains with an even number of carbons ranging from 16 to 26 in length (i.e. d18:1/16:0 through to d18:1/26:0), in the collated hippocampus extracts. The RT values were compared to those observed with the commercially available standards (d18:1/16:0 and d18:1/18:0 for GalCer; d18:1/16:0, d18:1/22:0, and d18:1/24:0 for SM), to confirm that the RT values were accurate to within 0.1 min. The six data points obtained from the hippocampus extracts were then fitted to a centered second order polynomial ($R^2 = 0.9992$ and 0.9993, for GalCer and SM, respectively) and relative RT values were obtained by fitting all observed *m/z* values to the equation and subtracting the resultant theoretical RT from the observed RT, as described above. Peak areas for each lipid identified were expressed as ratios to the relevant internal standard (d18:1/12:0 SM, d18:1/17:0 ceramide, or d18:1/12:0 GalCer), and normalized for the amount of starting brain tissue. For peaks identified by the *m/z* 264 product ion, the data was normalized separately to both ceramide and GalCer internal standards, yielding two distinct intensity plots.

Ceramide and GalCer content (in pmoles/mg tissue) was calculated from standard curves constructed with available synthetic standards. In the case of GalCer, standards for d18:1/18:0 and d18:1/24:0 GalCer were used to quantify long chain (C16 – C20) and very long chain (C22 – C26) GalCer, respectively.

Statistical Analysis

Two-tailed t-tests were used to compare lipid levels or ratios between normal and AD hippocampus, and between normal hippocampus and normal cerebellum. Equal variances were not assumed.

RESULTS

Mass and Relative Elution Time (MRET) profiling approach

In this article we use the LipidMAPS (www.lipidmaps.org) nomenclature system for sphingolipids, represented as "Lipid Class(length:double bonds of sphingoid base chain/length:double bonds of N-acyl chain)", e.g. SM(d18:1/24:0) refers to sphingomyelin with an 18-carbon sphingosine backbone with one double bond, and a 24-carbon N-acyl chain with no double bonds (Figure 1a).

The aim of this project was to create a system that facilitates the use of column RT, as well as precursor and product masses, for characterising the sphingolipid content of complex biological extracts. To define a relationship between mass and RT, we first used a mixture of ceramide standards. We observed that the elution, from a C8 column, of ceramide standards ranging in N-acyl chain length from 12 to 24 carbons follows a quadratic relationship under isocratic elution conditions (100% methanol) (Figure 1b). Using this equation, we calculated the theoretical RT for each of a mixture of ceramide and dihydroceramide standards. The difference between observed and theoretical RT was termed "relative RT", and plotted against *m/z* (Figure 1c). Ceramides differentiated only by the length of their N-acyl chain align horizontally, because they have an equivalent relative RT. Ceramides with an identical number of carbons but differing in the number of acyl chain double bonds align vertically. Ceramides with a 2-hydroxyl group in their N-acyl chain, referred to as Hydroxylated Fatty Acid (HFA) ceramides, are less hydrophobic and consequently have a more negative retention time relative to that expected for a Normal (i.e. non-hydroxylated) Fatty Acid (NFA) ceramide of equivalent mass. We next sought to determine if this approach would aid in the identification and characterization of sphingolipids in a complex biological extract.

Profiling the SM, Cer, and HexCer content of human brain tissue

De novo sphingolipid synthesis gives rise to ceramides, which are then used to produce SM, GalCer, and GluCer (Figure 1a). GluCer and GalCer are geometric isomers, and therefore can not be resolved on the basis of mass or affinity for the C8 column. GalCer is one of the major brain lipids, estimated to comprise 20 – 25 % of the total lipid content of myelin [23]. It is approximately 200-fold more abundant in the human brain than GluCer [24, 25], and we therefore refer to the human brain hexosylceramides that we have detected as GalCer, noting that this analyte is predicted to contain approximately 0.5 mol % GluCer.

We employed precursor ion scanning, using defined product ions with *m/z* 264 and 184, to identify the ceramide, GalCer, and SM species present in extracts of cerebellum and hippocampus from six AD patients, and six age- and gender-matched control subjects. The ion with *m/z* 264 is produced by sphingolipids with a d18:1 sphingosine backbone, whilst the ion with *m/z* 184 is the choline headgroup of SM. The LC-MS/MS data was processed as described in experimental procedures to generate a summary table showing *m/z* and RT values for all the distinct peaks in a set of samples, and the corresponding peak area (i.e. ion abundance) for that particular metabolite in each individual sample.

The principle SM, ceramide, and GalCer components in the cerebellum and hippocampus extracts are shown in Figure 2, in which the mean peak area (n = 6) relative to other lipids is represented by the size of the bubble. A colour gradient is used to show abundance in AD, relative to control brain extracts. Lipids with no double bonds in their N-acyl chain, but differing in the number of N-acyl chain carbons align horizontally with a relative RT of approximately 0. Lipids with an identical number of carbons but differing degrees of unsaturation align vertically, as exemplified by the alignment of ions on the SM maps with *m/z* 811.7, 813.7, and 815.7, representing d18:1/24:2, d18:1/24:1, or d18:1/24:0 SM, respectively (Figure 2a). To confirm the identity of these products as SM species with a sphingosine backbone, we verified that both 184 (phosphatidylcholine) and 264 (sphingosine backbone) *m/z* fragments were produced at the same column RT in a single sample run, after fragmentation of the *m/z* 731.6, 813.7, and 815.7 [SM(d18:1/18:0), SM(d18:1/24:1), and SM(d18:1/24:0)] precursor ions (collision energy 35 eV). Similarly, GalCer species with C24:1, C25:1, and C26:1 N-acyl chains (horizontal row at -1.0 to -1.1 min) align vertically with their C24:0, C25:0, and C26:0 counterparts (Figure 2c).

We identified two horizontal series of lipids whose mass corresponds to GalCer with a hydroxylated fatty acid (i.e. HFA-GalCer; +16 Da), and 0 or 1 double bonds in their N-acyl chain, indicated by long arrows in Figure 2c. These lipids cluster in terms of *m/z* and RT with other GalCer species, but as would be expected for HFA-GalCer, they elute from the C8 column earlier than their NFA counterparts, with relative RT of -1.1 to -1.4 (22:0, 23:0, 24:0, 25:0, 26:0 N-acyl chains) and -1.9 to -2.4 (23:1, 24:1, 25:1, 26:1 N-acyl chains), providing important evidence to confirm our prediction of their structure based on mass. Note that the shifted RT of these ions relative to their NFA counterparts also confirms that they are not oxidized GalCers, created during electrospray ionization. As expected, we observed no mass corresponding to the hydroxylated (*m/z* + 16) version of the GalCer(d18:1/12:0) internal standard. HFA lipids were observed only in GalCer, reflecting the strong preference of the enzyme UDP-galactose ceramide galactosyltransferase for HFA-ceramide substrates [26-28].

The importance of using relative RT for lipid identification is emphasized by the presence of two distinct peaks for *m/z* 826.7 indicated by arrowheads in Figure 2c. Using the online metabolomic search tool METLIN, this metabolite is identified as GalCer(d18:1/25:0). In accordance with that prediction, one of the peaks with *m/z* 826.7 has a relative RT of -0.07 and sits on the y-axis. However, the second peak has a relative RT of -2.17, and based on its position on the 2D plot, we predict that this ion is HFA-GalCer(d18:1/24:1). It aligns horizontally with 840.7 and 854.7 Da ions, which correspond by mass to HFA-GalCer with 25:1 and 26:1 N-acyl chains. Because GalCer(d18:1/25:0)

and HFA-GalCer(d18:1/24:1) are separated in mass by only 0.04 Da and generate the same product ion (*m/z* 264), they would probably have been misconstrued as the same lipid, using any mass spectrometer other than a very high mass accuracy instrument. To further verify that these are indeed distinct GalCer species, we checked their mass and relative elution pattern on an LTQXL Orbitrap: *m/z* for the earlier eluting peak, predicted to be HFA-GalCer(d18:1/24:1), was 826.6741 (predicted mass 826.6767, machine accuracy -3.13 ppm); whilst for the later eluting peak, predicted to be NFA-GalCer(d18:1/25:0), measured *m/z* was 826.7114 (predicted mass 826.7130, machine accuracy -1.99 ppm).

Another example further illustrates the importance of using relative RT in the identification of structure: in the ceramide plots an ion with *m/z* 664.6, indicated by an arrowhead in Figure 2e, could be either Cer(d18:1/25:0) or HFA-Cer(d18:1/24:1). Even in the absence of external standards for either of these lipids, we were readily able to identify this lipid as Cer(d18:1/25:0) based on its relative RT of 0.03 min.

Decreased total GalCer and increased HFA:NFA GalCer ratio in Alzheimer's Disease brains
Visual inspection of Figure 2f suggested that NFA-GalCer content declined by more than 2-fold in the hippocampus of AD patients, whilst HFA-GalCer was less affected. The reduction in GalCer content per mg tissue in AD hippocampus was in itself not statistically significant, due to the large standard deviations that are to be expected with human subjects ($P = 0.06$). However, when normalised to the SM content in each sample (thereby offsetting the variation in total lipid content between samples), the decline in GalCer levels in AD hippocampus was statistically significant (Figure 3a). Note that total hippocampus SM content was unchanged (control: 1.12 ± 0.25 nmoles/mg tissue; AD: 1.18 ± 0.24 nmoles/mg tissue (Mean ± Std Dev)). HFA-GalCer was significantly increased as a proportion of total GalCer (Figure 3b), and this altered HFA:NFA GalCer ratio was seen for all GalCer species (Figure 3c), suggesting either that fatty acid hydroxylase activity is increased or that catabolism of HFA-GalCer is slower than for NFA-GalCer in AD hippocampus. The only HFA-ceramide that could be detected was Cer(d18:1/24:0), which was present at detectable levels in all six of the AD hippocampus samples, but only one of the control samples. Having identified the major GalCer species present in human brain extracts using precursor ion scanning, we employed a more quantitative MRM approach to further test the utility of our relative elution time method and confirm the altered HFA:NFA-GalCer ratio in AD hippocampus.

Application of the relative elution time method to Multiple Reaction Monitoring experiments
Table 1 shows the MRM events we used and the specific species that we anticipated would be identified with each event. Figure 4a shows the total ion chromatogram for a single hippocampus sample, together with extracted ion chromatograms for the events with precursor ion *m/z* 826.7 or 840.7. As described above, the two peaks observed for the *m/z* 826.7 ion are NFA-GalCer(d18:1/25:0) and HFA-GalCer(d18:1/24:1), which are separated in mass by only 0.04 Da. There are no synthetic or purified standards for these lipids, so they can only be differentiated either through further fragmentation studies, or on the basis of their RT relative to known standards, as illustrated in Figure 4b. Similarly, two of the peaks observed in the *m/z* 840.7 event (Figure 4a) may be identified, based on their relative RT, as NFA-GalCer(d18:1/26:0) and HFA-GalCer(d18:1/25:1). The third, middle peak is a heavy isotope of NFA-GalCer(d18:1/26:1), which is removed by de-isotoping the data.

As was observed with precursor ion scanning, there was a reduction in the NFA-GalCer content of AD hippocampus, compared to the controls (Figure 4b and Table 1). All NFA-GalCers were reduced in abundance, in AD compared to control hippocampus samples, and there were statistically significant reductions in a number of very long chain ceramides (Table 1). In contrast, HFA-GalCer content did not decrease. Rather, there was a slight increase in total HFA-GalCer content, and calculation of the HFA-GalCer content as a proportion of total GalCer confirmed the statistical significance of this difference between control and AD subjects (Figure 4c).

Applicability of the relative elution time method to C18 chromatography

To demonstrate the portability of our method to other column types, we ran our mixture of ceramide and dihydroceramde standards and one of the hippocampus extracts on a C18 column, which are commonly used in sphingolipid analyses. As expected, the quadratic relationship between column RT and mass was also seen with this column (eluting under isocratic conditions with 100% methanol) (Figure 5a). The same relationship between RT and mass is observed when the ceramides are eluted with 90% isopropanol/10% water (data not shown). The pattern of hippocampal galactosylceramides eluting from the C18 column was very similar to that observed with a C8 column. Column RT for GalCer species with a sphingosine base and a saturated N-acyl chain (i.e. d18:1/N:0) followed a quadratic relationship with respect to mass, and after application of our RT transform the NFA-GalCer and HFA-GalCer species form distinct rows on a plot of relative RT vs *m/z* (Figure 5b).

DISCUSSION

The lipid profiling approach that we describe represents a significant improvement over current methods because the physicochemical characteristics of the lipids facilitate their identification. These characteristics may be critically important in resolving structurally different lipids that have almost identical mass and are within the same broad functional class, as in the example we present with NFA-GalCer(d18:1/25:0) and HFA-GalCer(d18:1/C24:1). Approaches that employ the physicochemical characteristics of lipids, including multi-dimensional mass spectrometry (MDMS)-based shotgun lipidomics [29] and TLC-MALDI [30], have been employed to separate different classes of lipids before MS analysis, but not to separate lipids within the same structural class. In fact, shotgun approaches such as MDMS are unable to resolve HFA- and NFA-GalCers that have almost identical mass [31]. The relative RT method that we describe herein greatly aids in the identification of lipids within the same structural class and in determining whether a particular metabolite belongs to a particular lipid class. We note that current published protocols for comprehensive sphingolipidomic analysis do not incorporate monitoring of HFA-GalCer [11, 12]. Although we employed a high mass accuracy Orbitrap instrument to verify our method, the use of these instruments is inherently more complex and they can not be set to perform precursor ion scans with defined product ions or multiple reaction monitoring.

In addition to improving the accuracy of lipid structure characterization, the resultant 2D plots greatly improve visualization of the data, when compared to a tabulated list. A recent review identified visualization of data as one of the key issues in sphingolipidomic systems analysis [1]. To illustrate this point, a 2D map of the MS intensity output using precursor ion scanning over the *m/z* range 680 – 900 (product ion *m/z* 264), from a single cerebellum sample before and after RT transformation is shown in Supplementary Figure 1. Plotting distinct LC peaks (as in Figure 2) rather than the raw intensity data (Supplementary Figure 1) improves the visual appearance of the data and makes it much simpler to present the mean of multiple samples, thereby improving our capacity to draw meaningful inferences from the data. Using our method, we could readily visualize the GalCer content of brain samples taken from AD patients and normal controls. Synthetic or purified standards are not available for most of the GalCer species shown in Figures 2 and 4, which makes the unambiguous assignment of lipid structure based on the most commonly employed MS^1 or MS^2 approaches impossible. More detailed analyses of the fragmentation pattern of individual lipids generally reveals the structure, but this is not always the case and this approach often necessitates chemical derivatization of lipids prior to MS analysis or the use of more reactive collision gases [32]. Using our approach, chemical derivatization is not necessary and important biochemical information can be obtained for many lipids simultaneously.

It is well established in the literature that precursor ion scanning, because of its reduced duty cycle, is less quantitative than MRM approaches. However, we believe that precursor ion scans such as we have used in this study are an important tool for establishing the principal lipids of interest for

subsequent MRM experiments, and are a valid approach for establishing trends in the data. We found that the principal trends observed using precursor ion scanning - a reduction in total GalCer content and an increase in HFA-GalCer content as a proportion of the total GalCer content - were reproduced in MRM mode which, as expected, yielded a greater linear range for absolute quantification. Although ceramide 1-phosphates were not abundant in the brain tissues analyzed in this study, we have found that the precursor ion scan with product ion *m/z* 264 used in this study is also sufficient to detect gross changes in ceramide 1-phosphate content in cultured cells. We have been unable to detect the principle dihydroceramide species using precursor ion scanning coupled to a product ion *m/z* of 266, due to their low abundance and their relatively poor fragmentation to the *m/z* 266 backbone ion (compared to the *m/z* 264 ion characteristic of sphingosine). However, we have found that sphingolipids bearing a sphinga-2,4-diene backbone can readily be identified with a precursor scan coupled to a product ion with *m/z* 262 (Supplementary Figure 1c) [33].

This is the first study to demonstrate an increase in the ratio of HFA-GalCer:NFA-GalCer in the brains of AD patients. This change was accompanied by an overall decline in hippocampal GalCer content, although not statistically significant in this study. The loss of GalCer in AD is in agreement with older literature employing thin layer chromatography techniques [34, 35]. These changes were observed in the hippocampus but not the cerebellum, in accordance with the pathology of AD: hippocampal atrophy associated with a pronounced loss of pyramidal neurons is a defining feature of AD, whilst the cerebellum is much less affected [36, 37]. More recent mass spectrometry analysis has shown a decline in sulfatide content, in the absence of any decline in GalCer content, in various regions of the cerebral cortex of AD subjects [38]. We note that these authors did not examine changes in the hippocampus, whilst we did not examine any frontal or temporal cortex tissue. In future studies, we aim to investigate the changes to these myelin sphingolipids using a much larger cohort of patient samples.

We found HFA-GalCer to comprise approximately 50% of total GalCer in the cerebellum, and 20% in the hippocampus of control subjects. Previous studies have reported that HFA-GalCer comprises approximately half of total GalCer in myelin [39, 40]. Whilst very long chain ceramides (those with >24 carbon N-acyl chains) declined in abundance in AD hippocampus, we observed an increase in the only detectible HFA-ceramide, d18:1/24:0 (Table 1). In precursor scanning mode, HFA-Cer(d18:1/24:0) was detected in all six AD hippocampus samples, but only one of the control hippocampus samples. These results suggest increased fatty acid hydroxylase activity in AD. Barrier et al [41] have very recently reported an increase in the ratio of HFA-ceramide:NFA-ceramide in the cerebral cortex, in a mouse model of AD (APP^{SL}/PS1 Ki). Interestingly, the increased ratio was only observed in female mice. Our human cohort is too small to draw firm conclusions on sex-related differences (see Table 2), but we note that when separated on the basis of gender, the HFA:NFA GalCer ratio was significantly different between AD and control females ($P = 0.0006$), but not males.

In summary, a rapidly growing body of literature is now highlighting the importance of lipid metabolites to cell signaling and pathophysiological processes. We present a new method that improves the combined use of liquid chromatography and mass spectrometry to create a 2D analysis of sphingolipids in a complex biological extract. The data transform that we apply can in theory be applied to any chromatography in which the separation of different lipids within the same functional class is dependent on the length of the lipid tails. The increased capacity of our approach to objectively profile lipid content is illustrated with the new findings we describe regarding changes in the sphingolipid content in the brains of AD patients. Our approach can be applied to other classes of lipids, and its application in lipidomics will improve the discovery process.

AUTHOR CONTRIBUTIONS

L.H. initiated the idea of LC×MS/MS, and contributed to method development, experimental work, and data analysis. J.W.H.W. contributed to method development, and extracted and collated peak

information from the LC-MS/MS raw data files; D.C. prepared human brain samples; N.P. contributed data analysis and advice; D.E. contributed to method development and data analysis; B.G. contributed to study design, data analysis, and interpretation; A.S.D. contributed to method development and study design, performed experimental work and data analysis, and wrote the manuscript, with contributions from L.H., J.W.H.W., D.E. and B.G.

ACKNOWLEDGEMENTS

We gratefully acknowledge the help of staff within the Bioanalytical Mass Spectrometry Facility at UNSW. We acknowledge the Sydney Brain Bank and the New South Wales Tissue Resource Centre, which are both part of the Australian Brain Bank Network, for provision of human brain tissues.

FUNDING

Funding Support: J.W.H.W. is supported by a UNSW Vice Chancellor's Fellowship. D.C. is supported by a PhD scholarship from the Australian Brain Foundation. D.E. is supported by a National Health and Medical Research Council training fellowship. B.G. is supported by an Australian Research Council Future Fellowship (FT0991986). A.S.D. is supported by a grant from the Cancer Institute NSW (08/ECF/1-03).

REFERENCES

1 Merrill, A. H., Jr., Stokes, T. H., Momin, A., Park, H., Portz, B. J., Kelly, S., Wang, E., Sullards, M. C. and Wang, M. D. (2009) Sphingolipidomics: a valuable tool for understanding the roles of sphingolipids in biology and disease. J Lipid Res. **50 Suppl**, S97-102

2 Hannun, Y. A. and Obeid, L. M. (2008) Principles of bioactive lipid signalling: lessons from sphingolipids. Nat Rev Mol Cell Biol. **9**, 139-150

3 Li, X., Becker, K. A. and Zhang, Y. (2010) Ceramide in redox signaling and cardiovascular diseases. Cell Physiol Biochem. **26**, 41-48

4 Frangioudakis, G., Garrard, J., Raddatz, K., Nadler, J. L., Mitchell, T. W. and Schmitz-Peiffer, C. (2010) Saturated- and n-6 polyunsaturated-fat diets each induce ceramide accumulation in mouse skeletal muscle: reversal and improvement of glucose tolerance by lipid metabolism inhibitors. Endocrinology. **151**, 4187-4196

5 Sidransky, E., Nalls, M. A., Aasly, J. O., Aharon-Peretz, J., Annesi, G., Barbosa, E. R., Bar-Shira, A., Berg, D., Bras, J., Brice, A., Chen, C. M., Clark, L. N., Condroyer, C., De Marco, E. V., Durr, A., Eblan, M. J., Fahn, S., Farrer, M. J., Fung, H. C., Gan-Or, Z., Gasser, T., Gershoni-Baruch, R., Giladi, N., Griffith, A., Gurevich, T., Januario, C., Kropp, P., Lang, A. E., Lee-Chen, G. J., Lesage, S., Marder, K., Mata, I. F., Mirelman, A., Mitsui, J., Mizuta, I., Nicoletti, G., Oliveira, C., Ottman, R., Orr-Urtreger, A., Pereira, L. V., Quattrone, A., Rogaeva, E., Rolfs, A., Rosenbaum, H., Rozenberg, R., Samii, A., Samaddar, T., Schulte, C., Sharma, M., Singleton, A., Spitz, M., Tan, E. K., Tayebi, N., Toda, T., Troiano, A. R., Tsuji, S., Wittstock, M., Wolfsberg, T. G., Wu, Y. R., Zabetian, C. P., Zhao, Y. and Ziegler, S. G. (2009) Multicenter analysis of glucocerebrosidase mutations in Parkinson's disease. N Engl J Med. **361**, 1651-1661

6 Haughey, N. J., Bandaru, V. V., Bae, M. and Mattson, M. P. (2010) Roles for dysfunctional sphingolipid metabolism in Alzheimer's disease neuropathogenesis. Biochim Biophys Acta. **1801**, 878-886

7 Krishnamurthy, K., Wang, G., Silva, J., Condie, B. G. and Bieberich, E. (2007) Ceramide regulates atypical PKCzeta/lambda-mediated cell polarity in primitive ectoderm cells. A novel function of sphingolipids in morphogenesis. J Biol Chem. **282**, 3379-3390

8 Wang, G., Krishnamurthy, K., Umapathy, N. S., Verin, A. D. and Bieberich, E. (2009) The carboxyl-terminal domain of atypical protein kinase Czeta binds to ceramide and regulates junction formation in epithelial cells. J Biol Chem. **284**, 14469-14475

9 Coetzee, T., Fujita, N., Dupree, J., Shi, R., Blight, A., Suzuki, K. and Popko, B. (1996) Myelination in the absence of galactocerebroside and sulfatide: normal structure with abnormal function and regional instability. Cell. **86**, 209-219

10 Dupree, J. L., Coetzee, T., Blight, A., Suzuki, K. and Popko, B. (1998) Myelin galactolipids are essential for proper node of Ranvier formation in the CNS. J Neurosci. **18**, 1642-1649

11 Bielawski, J., Pierce, J. S., Snider, J., Rembiesa, B., Szulc, Z. M. and Bielawska, A. (2009) Comprehensive quantitative analysis of bioactive sphingolipids by high-performance liquid chromatography-tandem mass spectrometry. Methods Mol Biol. **579**, 443-467

12 Shaner, R. L., Allegood, J. C., Park, H., Wang, E., Kelly, S., Haynes, C. A., Sullards, M. C. and Merrill, A. H., Jr. (2009) Quantitative analysis of sphingolipids for lipidomics using triple quadrupole and quadrupole linear ion trap mass spectrometers. J Lipid Res. **50**, 1692-1707

13 Chua, C. W., Lee, D. T., Ling, M. T., Zhou, C., Man, K., Ho, J., Chan, F. L., Wang, X. and Wong, Y. C. (2005) FTY720, a fungus metabolite, inhibits in vivo growth of androgen-independent prostate cancer. Int J Cancer. **117**, 1039-1048

14 Welthagen, W., Mitschke, S., Muhlberger, F. and Zimmermann, R. (2007) One-dimensional and comprehensive two-dimensional gas chromatography coupled to soft photo ionization time-of-flight mass spectrometry: a two- and three-dimensional separation approach. J Chromatogr A. **1150**, 54-61

15 Hejazi, L., Ebrahimi, D., Guilhaus, M. and Hibbert, D. B. (2009) Determination of the composition of fatty acid mixtures using GC x FI-MS: a comprehensive two-dimensional separation approach. Anal Chem. **81**, 1450-1458

16 Tew, N. (2010) Characterisation of Fatty Acid Methyl Esters (FAMEs) in Biodiesel using Liquid Chromatography - Mass Spectrometry (LC-MS) with Chemometrics. In School of Chemistry ed.)^eds.), University of New South Wales, Sydney
17 NIA. (1997) Consensus recommendations for the postmortem diagnosis of Alzheimer's disease. The National Institute on Aging, and Reagan Institute Working Group on Diagnostic Criteria for the Neuropathological Assessment of Alzheimer's Disease. Neurobiol Aging. **18**, S1-2
18 Kim, W. S., Bhatia, S., Elliott, D. A., Agholme, L., Kagedal, K., McCann, H., Halliday, G. M., Barnham, K. J. and Garner, B. (2010) Increased ATP-binding cassette transporter A1 expression in Alzheimer's disease hippocampal neurons. J Alzheimers Dis. **21**, 193-205
19 Bielawski, J., Szulc, Z. M., Hannun, Y. A. and Bielawska, A. (2006) Simultaneous quantitative analysis of bioactive sphingolipids by high-performance liquid chromatography-tandem mass spectrometry. Methods. **39**, 82-91
20 Keller, A., Eng, J., Zhang, N., Li, X. J. and Aebersold, R. (2005) A uniform proteomics MS/MS analysis platform utilizing open XML file formats. Mol Syst Biol. **1**, 2005 0017
21 Savitzky, A. and Golay, M. J. E. (1964) Smoothing + Differentiation of Data by Simplified Least Squares Procedures. Analytical Chemistry. **36**, 1627-&
22 Smith, C. A., Want, E. J., O'Maille, G., Abagyan, R. and Siuzdak, G. (2006) XCMS: processing mass spectrometry data for metabolite profiling using nonlinear peak alignment, matching, and identification. Anal Chem. **78**, 779-787
23 Norton, W. T. and Autilio, L. A. (1966) The lipid composition of purified bovine brain myelin. J Neurochem. **13**, 213-222
24 Vanier, M. T. and Svennerholm, L. (1975) Chemical pathology of Krabbe's disease. III. Ceramide-hexosides and gangliosides of brain. Acta Paediatr Scand. **64**, 641-648
25 Svennerholm, L., Vanier, M. T. and Mansson, J. E. (1980) Krabbe disease: a galactosylsphingosine (psychosine) lipidosis. J Lipid Res. **21**, 53-64
26 Shah, S. N. (1971) Glycosyl transferases of microsomal fractions from brain: synthesis of glucosyl ceramide and galactosyl ceramide during development and the distribution of glucose and galactose transferase in white and grey matter. J Neurochem. **18**, 395-402
27 Schaeren-Wiemers, N., van der Bijl, P. and Schwab, M. E. (1995) The UDP-galactose:ceramide galactosyltransferase: expression pattern in oligodendrocytes and Schwann cells during myelination and substrate preference for hydroxyceramide. J Neurochem. **65**, 2267-2278
28 van der Bijl, P., Strous, G. J., Lopes-Cardozo, M., Thomas-Oates, J. and van Meer, G. (1996) Synthesis of non-hydroxy-galactosylceramides and galactosyldiglycerides by hydroxy-ceramide galactosyltransferase. Biochem J. **317 (Pt 2)**, 589-597
29 Han, X. (2010) Multi-dimensional mass spectrometry-based shotgun lipidomics and the altered lipids at the mild cognitive impairment stage of Alzheimer's disease. Biochim Biophys Acta. **1801**, 774-783
30 Fuchs, B., Schiller, J., Suss, R., Zscharnack, M., Bader, A., Muller, P., Schurenberg, M., Becker, M. and Suckau, D. (2008) Analysis of stem cell lipids by offline HPTLC-MALDI-TOF MS. Anal Bioanal Chem. **392**, 849-860
31 Cheng, H., Jiang, X. and Han, X. (2007) Alterations in lipid homeostasis of mouse dorsal root ganglia induced by apolipoprotein E deficiency: a shotgun lipidomics study. J Neurochem. **101**, 57-76
32 Poad, B. L., Pham, H. T., Thomas, M. C., Nealon, J. R., Campbell, J. L., Mitchell, T. W. and Blanksby, S. J. (2010) Ozone-induced dissociation on a modified tandem linear ion-trap: observations of different reactivity for isomeric lipids. J Am Soc Mass Spectrom. **21**, 1989-1999
33 Colsch, B., Afonso, C., Popa, I., Portoukalian, J., Fournier, F., Tabet, J. C. and Baumann, N. (2004) Characterization of the ceramide moieties of sphingoglycolipids from mouse brain by ESI-MS/MS: identification of ceramides containing sphingadienine. J Lipid Res. **45**, 281-286
34 Svennerholm, L. and Gottfries, C. G. (1994) Membrane lipids, selectively diminished in Alzheimer brains, suggest synapse loss as a primary event in early-onset form (type I) and demyelination in late-onset form (type II). J Neurochem. **62**, 1039-1047
35 Wallin, A., Gottfries, C. G., Karlsson, I. and Svennerholm, L. (1989) Decreased myelin lipids in Alzheimer's disease and vascular dementia. Acta Neurol Scand. **80**, 319-323

36 West, M. J., Coleman, P. D., Flood, D. G. and Troncoso, J. C. (1994) Differences in the pattern of hippocampal neuronal loss in normal ageing and Alzheimer's disease. Lancet. **344**, 769-772
37 Braak, H. and Braak, E. (1995) Staging of Alzheimer's disease-related neurofibrillary changes. Neurobiol Aging. **16**, 271-278; discussion 278-284
38 Han, X., D, M. H., McKeel, D. W., Jr., Kelley, J. and Morris, J. C. (2002) Substantial sulfatide deficiency and ceramide elevation in very early Alzheimer's disease: potential role in disease pathogenesis. J Neurochem. **82**, 809-818
39 Eng, L. F., Gerstl, B., Hayman, R. B., Lee, Y. L., Tietsort, R. W. and Smith, J. K. (1965) The 2-Hydroxy Fatty Acids in White Matter of Infant and Adult Brains. J Lipid Res. **6**, 135-139
40 Blass, J. P. (1970) Fatty acid composition of cerebrosides in microsomes and myelin of mouse brain. J Neurochem. **17**, 545-549
41 Barrier, L., Ingrand, S., Fauconneau, B. and Page, G. (2010) Gender-dependent accumulation of ceramides in the cerebral cortex of the APP(SL)/PS1Ki mouse model of Alzheimer's disease. Neurobiol Aging. **31**, 1843-1853

TABLES

Table 1. Abundance of individual ceramide and GalCer species in human hippocampus extracts, as determined by MRM.

Lipids possess non-hydroxylated fatty acid (NFA) chains, unless HFA is prefixed to the name. Different lipids sharing the same precursor mass were differentiated on the basis of relative RT. The product *m/z* was set at 264.1 for all events, whilst collision energy was set at 30 eV for ceramides and 35 eV for GalCers. Note that internal standards Cer(d18:1/17:0) and GalCer(d18:1/12:0) were detected with precursor *m/z* 552.7 and 644.6, respectively. Units of abundance are pmoles lipid/mg tissue, and values shown are the mean ± standard deviation of six patient samples. Dash indicates that lipid was not quantified due to very low abundance. Asterisk (*) indicates a statistically significant difference ($P < 0.05$) between control and AD hippocampus, as determined by two-tailed t-test.

Lipid	Precursor m/z	Abundance Control Hippocampus	Abundance AD Hippocampus
Cer(d18:1/16:0)	538.6	0.30 ± 0.15	0.52 ± 0.23
Cer(d18:1/18:1)	564.6	-	-
Cer(d18:1/18:0)	566.7	6.44 ± 2.46	6.43 ± 4.31
Cer(d18:1/20:0)	594.7	0.12 ± 0.033	0.18 ± 0.10
Cer(d18:1/22:0)	622.7	0.10 ± 0.040	0.098 ± 0.022
Cer(d18:1/23:1)	634.7	-	-
Cer(d18:1/23:0)	636.7	0.097 ± 0.042	0.060 ± 0.022
Cer(d18:1/24:1)	648.8	2.81 ± 1.11	1.52 ± 0.83*
Cer(d18:1/24:0)	650.8	0.27 ± 0.14	0.15 ± 0.068
Cer(d18:1/25:1)	662.8	0.55 ± 0.27	0.23 ± 0.15*
Cer(d18:1/25:0)	664.8	0.043 ± 0.026	0.015 ± 0.0098*
HFA-Cer(d18:1/24:0)	666.8	0.0089 ± 0.0084	0.0139 ± 0.0062
Cer(d18:1/26:1)	676.8	0.25 ± 0.096	0.081 ± 0.051*
Cer(d18:1/26:0)	678.8	-	-
Total Ceramide		10.96 ± 3.14	9.28 ± 4.92
GalCer(d18:1/16:0)	700.7	3.00 ± 1.82	2.08 ± 1.31
GalCer(d18:1/18:1)	726.7	-	-
GalCer(d18:1/18:0)	728.7	184.5 ± 89.5	106.2 ± 120.9
HFA-GalCer(d18:1/18:1)	742.7	-	-
HFA-GalCer(d18:1/18:0)	744.7	7.38 ± 3.25	5.98 ± 3.68
GalCer(d18:1/20:1)	754.7	-	-
GalCer(d18:1/20:0)	756.7	10.97 ± 3.73	7.16 ± 8.59
HFA-GalCer(d18:1/20:1)	770.7	-	-
HFA-GalCer(d18:1/20:0)	772.7	-	-
GalCer(d18:1/22:1)	782.7	6.87 ± 2.73	4.06 ± 4.65
GalCer(d18:1/22:0)	784.7	39.95 ± 13.83	26.82 ± 24.85
GalCer(d18:1/23:1)	796.7	22.91 ± 10.24	11.51 ± 12.36
GalCer(d18:1/23:0)	798.7	64.11 ± 20.91	40.89 ± 27.20
HFA-GalCer(d18:1/22:1)	798.7	-	-
HFA-GalCer(d18:1/22:0)	800.7	23.48 ± 9.99	28.21 ± 9.06
GalCer(d18:1/24:1)	810.7	685.3 ± 291.1	387.9 ± 366.6
GalCer(d18:1/24:0)	812.7	247.5 ± 85.6	155.8 ± 106.8
HFA-GalCer(d18:1/23:1)	812.7	-	-

HFA-GalCer(d18:1/23:0)	814.7	34.06 ± 18.47	47.20 ± 18.74
GalCer(d18:1/25:1)	824.8	202.4 ± 84.7	122.1 ± 89.7
GalCer(d18:1/25:0)	826.8	85.77 ± 28.99	56.96 ± 43.49
HFA-GalCer(d18:1/24:1)	826.8	168.1 ± 70.0	142.6 ± 50.1
HFA-GalCer(d18:1/24:0)	828.8	53.80 ± 28.07	67.57 ± 33.13
GalCer(d18:1/26:1)	838.8	208.5 ± 57.9	126.5 ± 66.1*
GalCer(d18:1/26:0)	840.8	30.21 ± 7.70	20.02 ± 17.30
HFA-GalCer(d18:1/25:1)	840.8	19.81 ± 12.67	32.22 ± 16.82
HFA-GalCer(d18:1/25:0)	842.8	14.70 ± 8.28	21.17 ± 8.54
HFA-GalCer(d18:1/26:1)	854.8	21.55 ± 10.65	40.33 ± 23.28
HFA-GalCer(d18:1/26:0)	856.8	9.57 ± 3.38	8.50 ± 3.79
Total Galcer		2145 ± 741	1462 ± 888
Total NFA-GalCer		1792 ± 613	1068 ± 860
Total HFA-GalCer		352.5 ± 148.6	393.7 ± 135.5

Table 2. Patient brain samples used in this study
PMI, post-mortem interval; NFT, neurofibrillary tangle

ID#	age	gender	PMI (hrs)	cause of death	disease duration (yrs)	Braak NFT stage [37]
1	85	female	23	pneumonia	0	0
2	79	male	8	pulmonary embolism	0	0
3	93	female	21	cardiac failure	0	0
4	78	female	11	respiratory failure	0	0
5	69	male	13.5	myocardial infarction	0	0
6	82	male	23.5	multiple organ failure	0	0
7	83	male	25	cerebrovascular accident	5	stage VI
8	84	female	6	aspiration pneumonia	13	stage VI
9	83	female	3	uraemia	7	stage V
10	73	male	16	bronchopneumonia	11	stage VI
11	83	female	4	circulatory collapse	9	stage V
12	69	male	3	colon cancer	5	stage VI

FIGURE LEGENDS

Figure 1. Two dimensional separation of ceramide standards according to mass and hydrophobicity. (a) Structure and biochemical relationship of SM, ceramide, and GalCer. (b) Plot of RT against *m/z* for a mixture of 16 different ceramide (Cer) and dihydroceramide (dhCer) standards, as analysed by LC-MS/MS (10 pmole each). Lipids were separated on a C8 column and individual species were identified by precursor ion scanning, monitoring for 264 and 266 Da product ions, at 30 eV. The curve is a centered second order polynomial, fitted to the following 7 standards: d18:1/12:0 (C12:0 Cer), d18:1/14:0 (C14:0 Cer), d18:1/16:0 (C16:0 Cer), d18:1/18:0 (C18:0 Cer), d18:1/20:0 (C20:0 Cer), d18:1/22:0 (C22:0 Cer), and d18:1/24:0 (C24:0 Cer). The other standards shown are: d18:0/16:0 (C16:0 dhCer), d18:0/18:0 (C18:0 dhCer), d18:0/24:0 (C24:0 dhCer), d18:0/18:1 (C18:1 dhCer); d18:0/C24:1 (C24:1 dhCer); d18:1/18:1 (C18:1 Cer); d18:1/24:1 (C24:1 Cer); d18:1/18:0(2-OH) (C18:0 HFA-Cer) and d18:1/24:0(2-OH) (C24:0 HFA-Cer). (c) Relative RT plotted against *m/z* for all 16 standards. The identity of each standard is indicated on the graph. Note the vertical alignment of standards with equivalent or almost equivalent mass, but a different number or position of double bonds, indicative of separation based on hydrophobicity.

Figure 2. 2D plots of sphingolipid content in cerebellum and hippocampus: comparison of control to AD brains. SM (a and d), ceramide (b and e), and GalCer (c and f) content of cerebellum (a-c) and hippocampus (d-f). Each bubble represents a distinct ion peak on a plot of relative RT vs *m/z*, and the size of the bubble is indicative of peak area after adjusting for internal standard recovery and mass of homogenized tissue. Bubble sizes shown (i.e. adjusted peak areas) are the mean of six samples, and for clarity in presentation, the sizing of the bubbles is normalized within each functional class, i.e. SM, Cer and GalCer. The colour gradient indicates intensity of that metabolite in AD samples (mean of 6), relative to control (mean of 6). Red: increased in AD; Blue: decreased in AD brains. Relative RT was derived by transformation of RT for each corresponding *m/z*, relative to SM, ceramide or GalCer with saturated N-acyl chains, as described in experimental procedures. C16, C18, C20, C22, C24, and C26 refer to the length of N-acyl chains, as determined by mass and referenced to external standards. Horizontal arrows show rows of HFA-GalCer species. Arrowheads in (c) indicate the position of two distinct bubbles with an *m/z* of 826.7, which are GalCer(d18:1/25:0), at Relative RT = 0; and HFA-GalCer(d18:1/24:1), at Relative RT = -2.2. Arrowhead in (e) indicates position of Cer(d18:1/25:0).

Figure 3. Decreased GalCer and increased GalCer hydroxylation in AD hippocampus. (a) Total GalCer content is expressed relative to total SM content in each of the brain samples. Horizontal bars show the mean (n = 6). (b) Scatter plots showing total HFA-GalCer peak area, as a proportion of total (HFA-GalCer + NFA-GalCer) peak area. (c) HFA-GalCer peak area, as a proportion of total (HFA-GalCer + NFA-GalCer) peak area, for each different N-acyl chain length. Values are mean ± standard error (n = 6). P values were derived from unpaired, two-tailed t-tests.

Figure 4. Use of relative elution time to confirm identity of GalCer species in MRM. (a) Total Ion Chromatogram (TIC) and extracted chromatograms for the *m/z* 826.7 and 840.7 events, for a hippocampus extract from a control patient analysed in MRM mode (events shown in Table 1). (b) Relative RT vs *m/z* plot showing GalCer peaks detected in MRM mode. Bubbles illustrate the relative abundance of each metabolite in all six control hippocampus extracts, and colour gradient describes the abundance of each metabolite in the six AD, relative to the control, hippocampus extracts. (c) HFA-GalCer as a proportion of total GalCer (HFA + NFA), for each of the control (n = 6) and AD (n = 6) hippocampus samples. P value was derived from a two-tailed t-test.

Figure 5. Application of relative elution time method with a C18 chromatography column. (a) Elution pattern for a mixture of ceramide standards eluted from a C18 column under isocratic conditions (100% methanol); (i) shows absolute RT; whilst (ii) shows relative RT. Using a C18 column, the relationship between *m/z* and RT fits a quadratic equation. (b) Relative RT vs *m/z* plot of the GalCer content in a control hippocampus extract, using a C18 chromatography column.

Figure 1

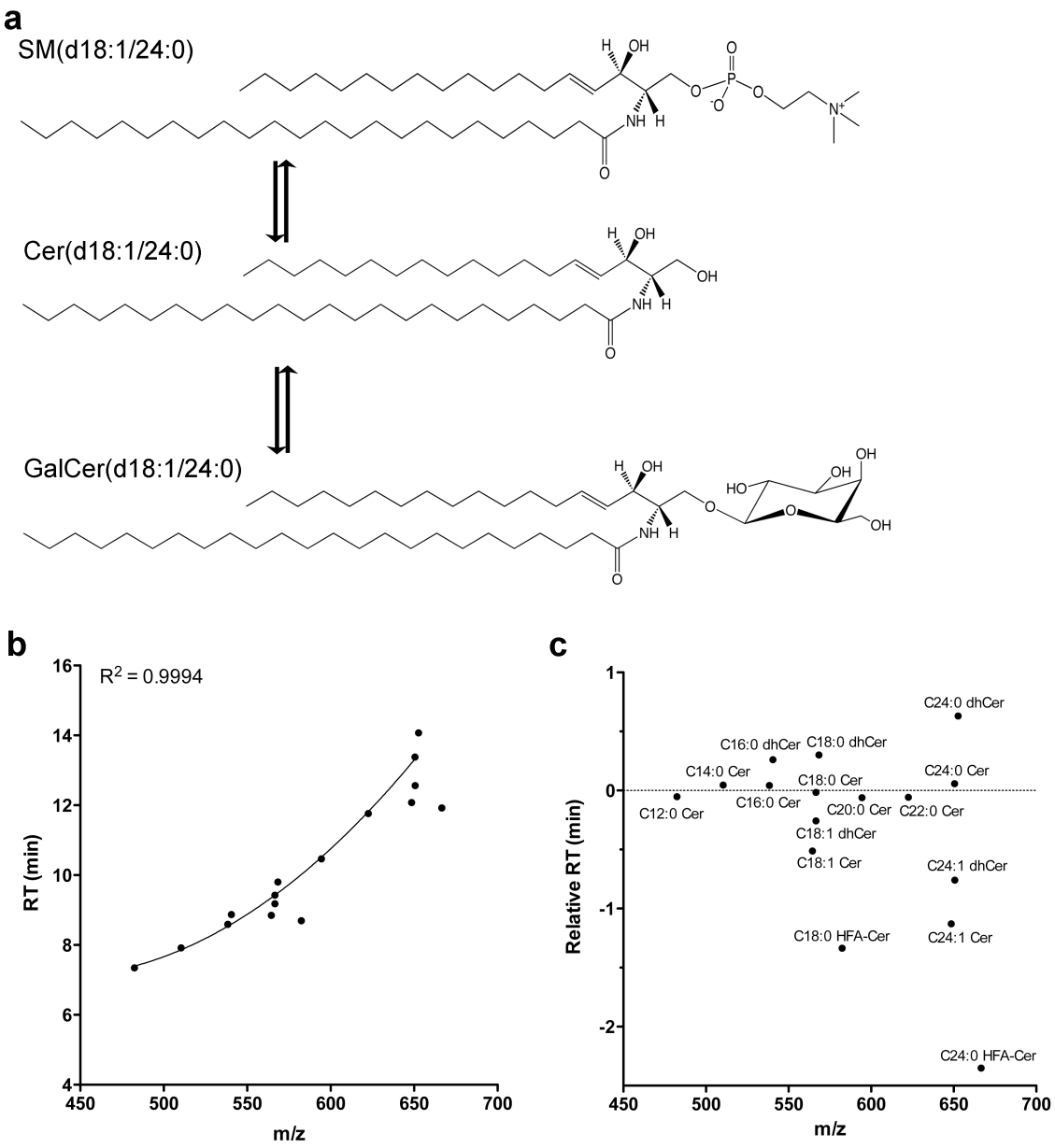
a
SM(d18:1/24:0)
Cer(d18:1/24:0)
GalCer(d18:1/24:0)
b
R2 = 0.9994
RT (min)
m/z
c
Relative RT (min)
m/z
C24:0 dhCer
C16:0 dhCer
C18:0 dhCer
C14:0 Cer
C18:0 Cer
C24:0 Cer
C12:0 Cer
C16:0 Cer
C20:0 Cer
C22:0 Cer
C18:1 dhCer
C18:1 Cer
C24:1 dhCer
C18:0 HFA-Cer
C24:1 Cer
C24:0 HFA-Cer

Figure 2

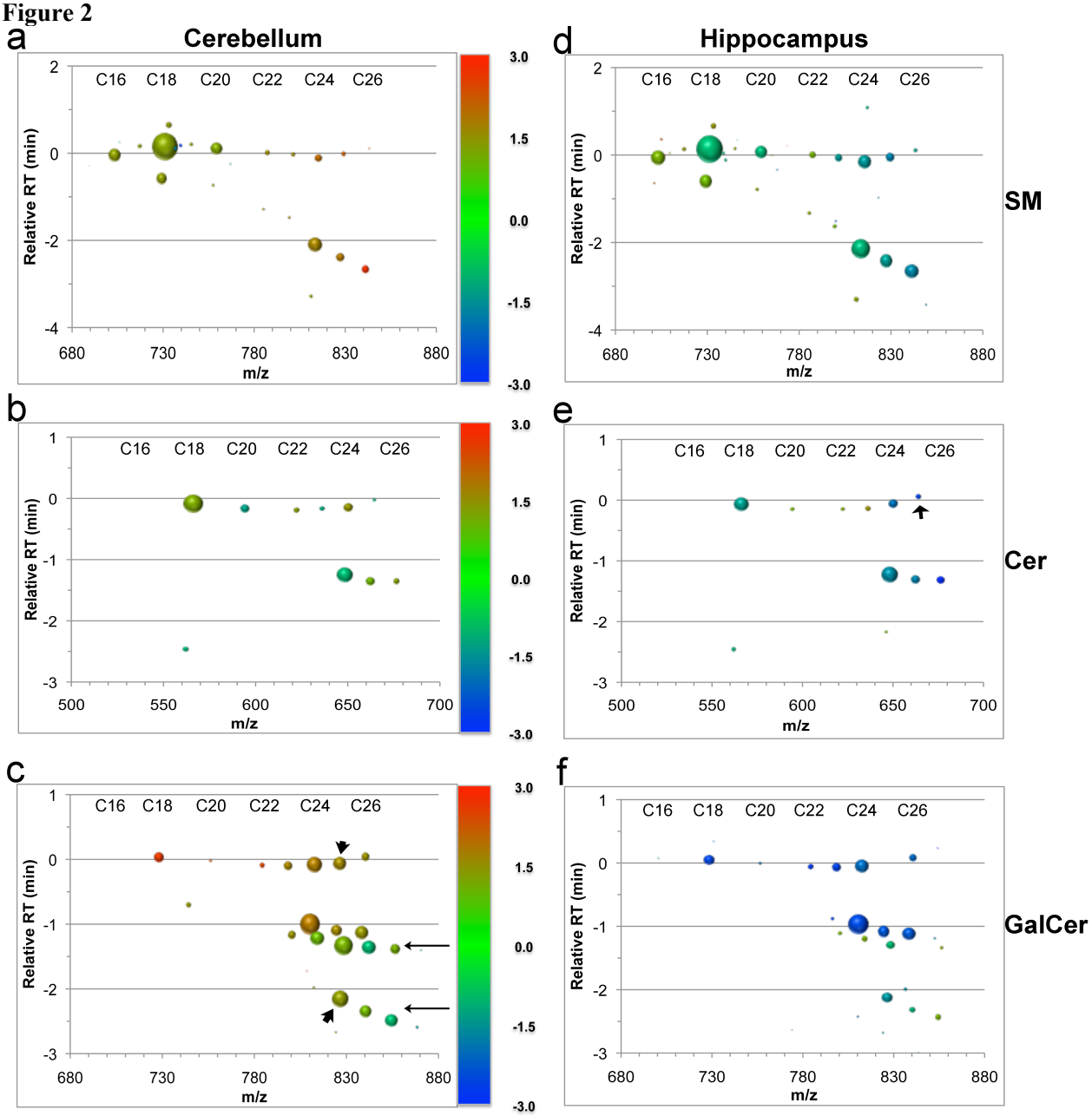
a
Cerebellum
d
Hippocampus
SM
b
e
Cer
c
f
GalCer
C16 C18 C20 C22 C24 C26
Relative RT (min)
m/z
3.0
1.5
0.0
-1.5
-3.0

Figure 3

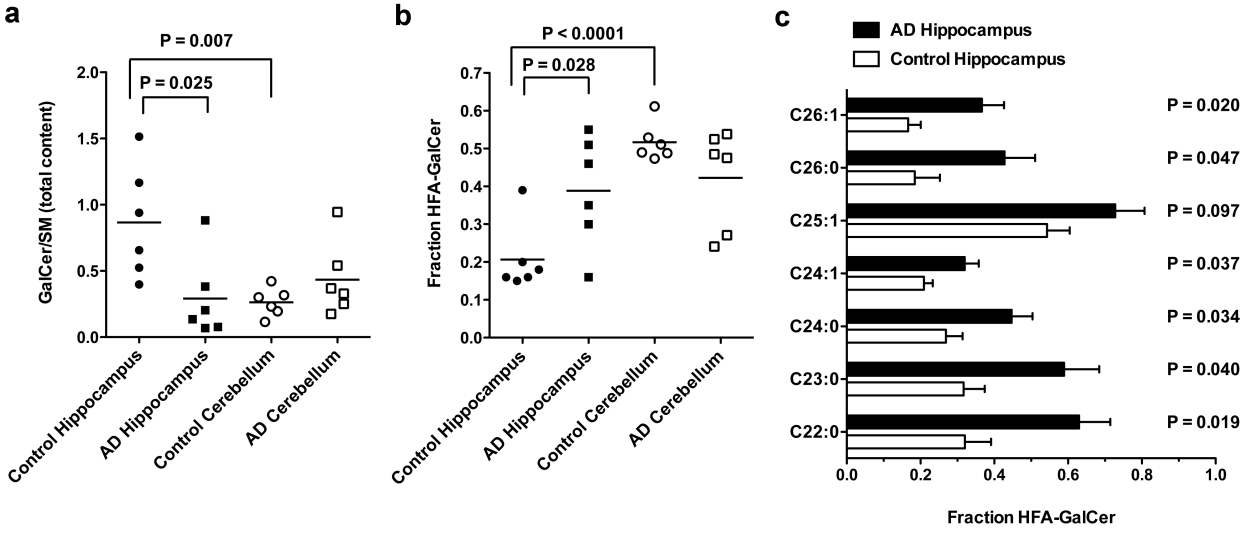
a
P = 0.007
P = 0.025
GalCer/SM (total content)
2.0
1.5
1.0
0.5
0.0
Control Hippocampus
AD Hippocampus
Control Cerebellum
AD Cerebellum
b
P < 0.0001
P = 0.028
Fraction HFA-GalCer
0.7
0.6
0.5
0.4
0.3
0.2
0.1
0.0
Control Hippocampus
AD Hippocampus
Control Cerebellum
AD Cerebellum
c
AD Hippocampus
Control Hippocampus
C26:1
C26:0
C25:1
C24:1
C24:0
C23:0
C22:0
P = 0.020
P = 0.047
P = 0.097
P = 0.037
P = 0.034
P = 0.040
P = 0.019
0.0
0.2
0.4
0.6
0.8
1.0
Fraction HFA-GalCer

Figure 4

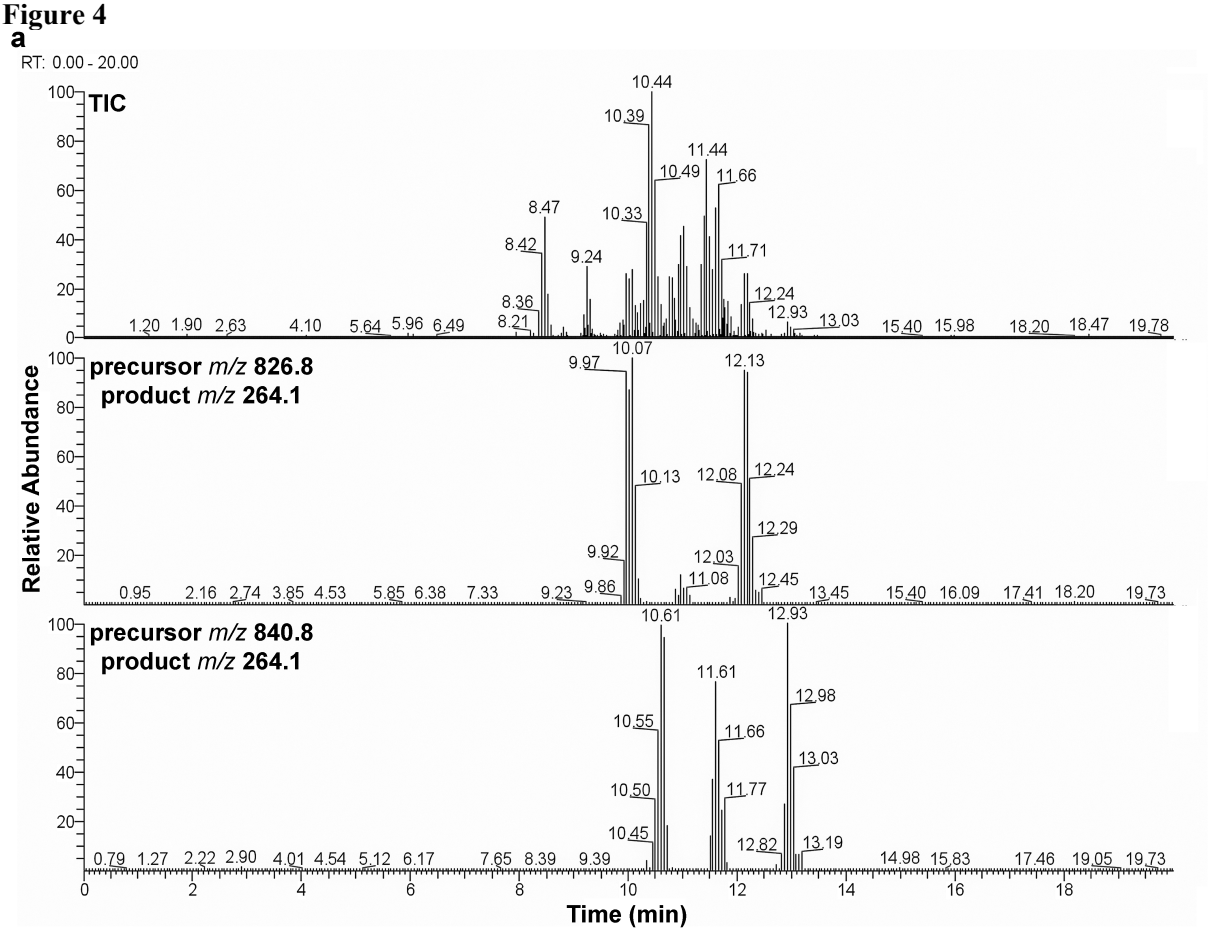
a
RT: 0.00 - 20.00
TIC
precursor m/z 826.8
product m/z 264.1
precursor m/z 840.8
product m/z 264.1
Relative Abundance
Time (min)

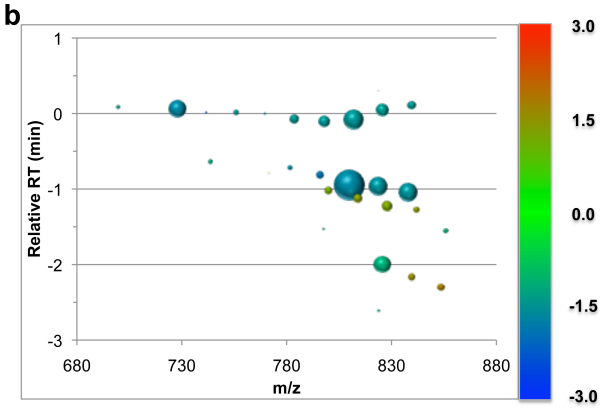
b
Relative RT (min)
m/z

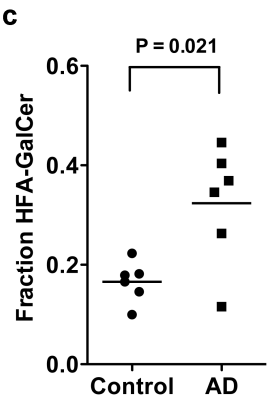
c
P = 0.021
Fraction HFA-GalCer
Control
AD

Figure 5

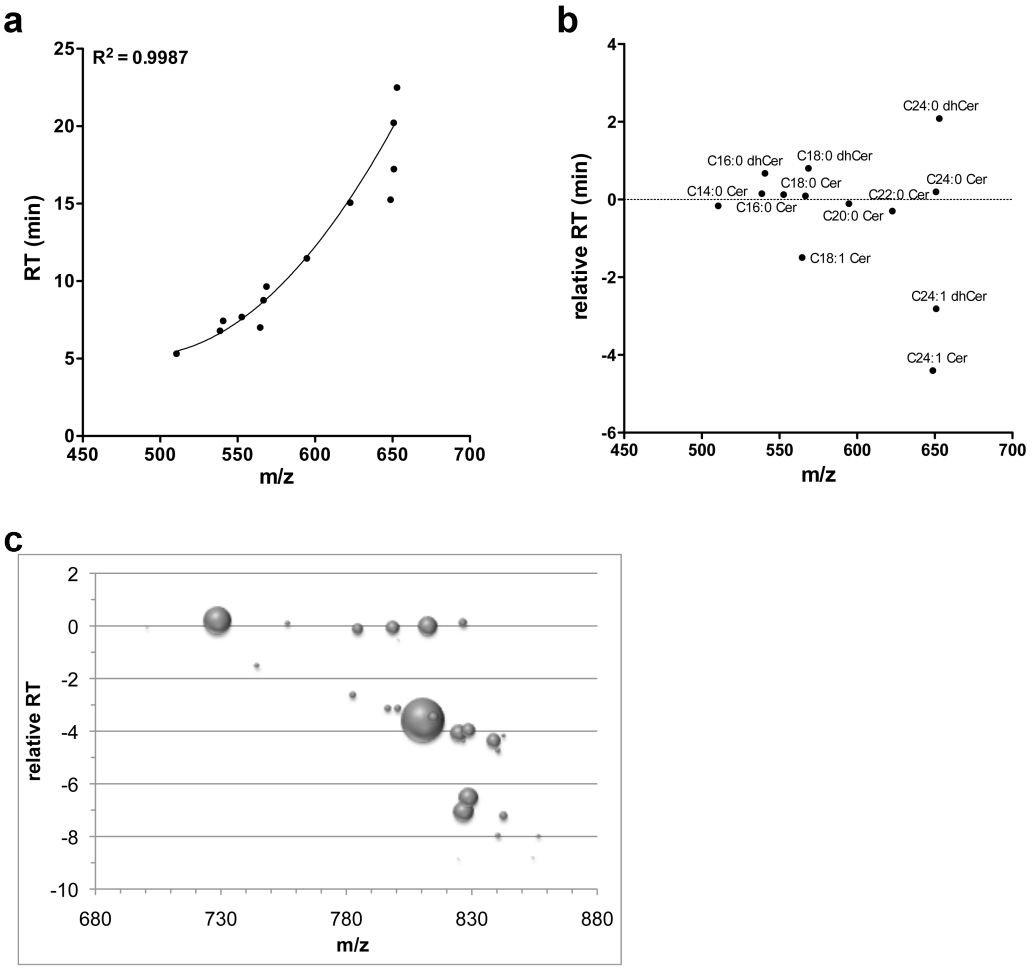
a
R² = 0.9987
RT (min)
m/z
b
relative RT (min)
m/z
C24:0 dhCer
C16:0 dhCer
C18:0 dhCer
C24:0 Cer
C18:0 Cer
C14:0 Cer
C22:0 Cer
C16:0 Cer
C20:0 Cer
C18:1 Cer
C24:1 dhCer
C24:1 Cer
c
relative RT
m/z